Journal of Nepal Mathematical Society (JNMS)
ISSN: 2616-0153 (Print), 2616-0161 (Online)
Vol. 8, Issue 2, 2025 (Dec.): 01-15
DOI: https://doi.org/10.3126/jnms.v8i2.87702

Research Article
Received Date: Aug. 21, 2025
Accepted Date: Nov. 24, 2025
Published Date: Dec. 29, 2025

Numerical Solutions of Second-Order Fractional Differential Equations: Atangana-Baleanu Caputo Fractional Derivative Approach

Jeevan Kafle[1], Kushal Poudel[1,4], Shankar Pariyar[1,2,*], Hem Raj Pandey[3]

[1]Central Department of Mathematics, Institute of Science and Technology, Tribhuvan University, Nepal
[2]Department of Mathematics, Tri-Chandra Multiple Campus, Nepal
[3]School of Engineering, Faculty of Science and Technology, Pokhara University, Nepal
[4]Himalayan WhiteHouse International College, Purvanchal University, Nepal

*Correspondence to: shankar.pariyar@trc.tu.edu.np

Abstract
In this work, we develop a numerical framework for solving second-order fractional differential equations.Second-order fractional differential equations involving the Atangana–Baleanu Caputo fractional derivative, which models nonlocal and memory-dependent dynamical behavior. The numerical scheme is constructed using Lagrange polynomial interpolation adapted to the Atangana–Baleanu Caputo operator. A rigorous convergence and stability analysis is carried out using a fixed-point (contraction) argument under a natural Lipschitz condition. The theoretical results are supported by several numerical experiments that cover linear and nonlinear test problems. The contribution of this study lies in the establishment of a stable and accurate ABC-based numerical scheme and the verification that it standardizes its performance across a wide range of source functions. In general, the proposed method appears to be a powerful and efficient tool for modeling and analyzing complex systems that obey fractional dynamics.

Keywords: Fractional differential equation, Numerical scheme, Lagrange's polynomial, Approximate solution.

1 Introduction

The derivative of fractional order in differential equations has the ability to capture and characterize the behaviors of complicated systems [31] and phenomena that are not well suited to description by integer-order differential equations [15, 23].Fractional differential equations (FDEs) naturally arise in systems governed by memory, hereditary effects, and non-local interactions, where classical integer-order models usually cannot represent the physical behavior accurately. The extended Kalman filter effectively approximates nonlinear behavior effectively [17, 22]. There are many definitions of fractional calculus, including the Riemann–Liouville (RL) fractional derivative, the Caputo fractional derivative [8], the Atangana–Baleanu Caputo (ABC) fractional derivative [17] and the Caputo–Fabrizio fractional derivative [20]. Fractional derivatives are generally classified into two categories: singular kernel and non-singular kernel types.Singular kernel operators (such as the RL and Caputo derivatives) incorporate power-law memory, while nonsingular kernel operators, such as the ABC and Caputo–Fabrizio derivatives, use smooth kernels that avoid algebraic singularities [7].

Leibniz mentions the derivative of a general order and uses differential calculus notation such as $d^{\frac{1}{2}}y$ for order 1/2 in his correspondence with John Wallis about Wallis's infinite product for $\frac{\pi}{2}$ [24]. A prominent mathematician in fractional calculus, Euler devised the gamma and beta functions [19].The foundational contributions of Abel, Riemann, Liouville, and Caputo later established the modern definitions of fractional integration and differentiation [23]. The historical development of fractional calculus continued through Lacroix and Laplace, and later through major international conferences in New Haven (1974) and Glasgow (1984), which gave tremendous impetus to modern research in this area [1, 2, 25]. Pariyar et al. and Pandey et al. [17, 19] investigated the effects of step size and fractional order on the smoothness and accuracy of solutions for certain special functions, illustrating the increased flexibility of fractional models. Atangana et al. [32] derived numerical schemes and error estimates for ABC fractional differential equations of the first order with non-singular nonlocal kernels.Qazza et al. [17] proposed new numerical methods for general

first-order fractional differential equations, highlighting the advantages of non-singular fractional operators [20].

In this work, we derive the approximate solution of the fractional differential equation (FDE) in the form [30]

$$\begin{cases} D^{\phi}(D^{\phi}\psi(z)) = h(z,\psi(z)), \\ D^{\phi}\psi(0) = \psi_1, \quad \psi(0) = \psi_0, \end{cases} \tag{1}$$

where D^{ϕ} denotes the Atangana–Baleanu fractional derivative in the Caputo sense (ABC derivative). Since obtaining closed-form analytical solutions for general FDEs is often impossible, constructing reliable approximate solutions becomes essential. Numerical and semi-analytical approaches are available for approximating solutions of FDEs, including Euler and Adams–Bashforth methods, the Adomian decomposition method, homotopy analysis, Laplace–Adomian decomposition methods [10], and polynomial interpolation techniques [17, 22]. In particular, second-order FDEs can be effectively approximated using Lagrange polynomial interpolation combined with the ABC operator. This framework provides a practical and efficient approximation solution. It also enables a direct comparison between approximate and exact solutions whenever the latter is available. Thus, the method is particularly desirable when it produces high accuracy and minimal error, especially for problems where analytical solutions cannot be obtained.

In this work, we demonstrate the efficacy of the proposed method using several two and three dimensional graphical representations of second-order fractional differential equations.It also demonstrates how the solutions for different values of the fractional-order index ϕ are related. We derive a numerical scheme to solve SOFDEs, which is applicable in various fields such as physics and engineering. This scheme efficiently and accurately solves the initial value problem using the ABC fractional derivative [18].The proposed numerical method is simple and straightforward to solve SOFDEs. The structure of this paper is as follows: Section 2 defines various fundamental terms, including the Lagrange polynomial, the ABC fractional derivative, and the Caputo fractional derivative. Section 3 presents a numerical technique using the Lagrange polynomial and ABC operator, followed by an alternative equation to determine the solution. Finally, we discuss the results and present the conclusion.

2 Some Basic Definitions

First, we define key terms such as the Riemann–Liouville fractional derivative and integral, the Caputo fractional integral, the Atangana–Baleanu Caputo fractional derivative, the Mittag–Leffler function (MLF), and Lagrange polynomial interpolation.

Definition 2.1 ([16])**.** For the function $\psi(z)$, the Riemann-Liouville (RL) fractional derivative of order ϕ satisfies the following condition for $\mu - 1 < \phi < \mu$;

$${}^{RL}D^{\phi}\psi(z) = \frac{d^{\mu}}{dz^{\mu}} I^{\mu-\phi}\psi(z) = \frac{1}{\Gamma(\mu-\phi)} \frac{d^{\mu}}{dz^{\mu}} \int_0^z \psi(\eta)\cdot(z-\eta)^{\mu-\phi-1}\, d\eta,\ \eta > 0. \tag{2}$$

where Γ is gamma function and $\psi^{\mu}(\eta)$ is m-order derivative.

Example. Let $\psi(z) = z^2$ and $\varphi = \frac{1}{2}$. Then the Riemann–Liouville fractional derivative is $D^{1/2}_{RL}\, z^2 = \frac{2}{\Gamma(5/2)}\, z^{3/2}$.

Definition 2.2 ([25])**.** For function $\psi(z)$, Riemann-Liouville fractional integral of order ϕ satisfying the condition

$${}_aI^{\phi}_z\psi(z) = \frac{1}{\Gamma(\phi)} \int_a^z \psi(\eta)\cdot(z-\eta)^{\phi-1}\, d\eta, \eta > a. \tag{3}$$

Example. For $\psi(z) = z$ and $\varphi = \frac{1}{2}$, the Riemann–Liouville fractional integral is $I^{1/2}_{0,z} z = \frac{2}{3}\, z^{3/2}$.

Definition 2.3 ([30])**.** For a given function $\psi(z)$, Caputo fractional integral of order ϕ satisfying the following condition for $0 < \phi < 1$

$$I^{\phi}\psi(z) = \frac{1}{\Gamma(\phi)} \int_0^z \psi(\eta)\cdot(z-\eta)^{\phi-1}\, d\eta, \eta > 0. \tag{4}$$

Example. Let $\psi(z) = \cos z$ and $\varphi = \frac{1}{2}$. Then the Caputo fractional integral is $I^{1/2}(t) = \frac{4}{3\sqrt{\pi}} t^{3/2}$.

Definition 2.4 ([11]). For a given function $\psi(z)$, Caputo fractional derivative of order ϕ satisfying condition

$$ {}_0D_z^{\phi}\psi(z) = \begin{cases} \frac{1}{\Gamma(\mu-\phi)} \int_0^z (\frac{d}{dz})^{\mu} \psi(\eta) \cdot (z-\eta)^{\mu-\phi-1} \, d\eta & \text{for } \mu - 1 < \phi < \mu, \\ \frac{d^{\mu}}{dz^{\mu}} \psi(z), & \text{for } \phi = \mu. \end{cases} \tag{5} $$

Example. For $\psi(z) = z^3$ and $\varphi = \frac{1}{2}$, the Caputo derivative is $D_C^{1/2} z^3 = \frac{6}{\Gamma(5/2)} z^{5/2}$.

Definition 2.5 ([20]). A Swedish mathematician who defined and researched the Mittag Leffler function in 1903 is honored with the function's name. For one parameter, it is denoted by E_p and defined as

$$ E_p(z) = \sum_{r=0}^{\infty} \frac{z^r}{\Gamma(pr+1)}. \tag{6} $$

For two parameters [22, 30], Mittag Leffler function is denoted by $E_{p,q}$ and defined as

$$ E_{p,q}(z) = \sum_{r=0}^{\infty} \frac{z^r}{\Gamma(pr+q)}. \tag{7} $$

Example. The Mittag–Leffler function with one parameter satisfies $E_1(z) = e^z$. For two parameters, $E_{1,1}(z) = e^z$.

Definition 2.6 ([19, 32]). Lagrange polynomial interpolation is a method for approximating a function by creating a polynomial that runs over points (y_0, y_1), (y_1, y_2), ...,$(y_{\mu-1}, y_{\mu})$ can be defined as

$$ P_m(y) = \sum_{j=0}^{\mu} g(y_j) L_j(y), $$

where

$$ L_j = \prod_{i=0, i\neq j}^{\mu} \frac{y - y_j}{y_j - y_i}. $$

Example. Given the points $(0, 1)$ and $(1, 2)$, the Lagrange interpolation polynomial is $P_1(z) = 1(1-z)+2z = 1 + z$.

Definition 2.7 ([17]). For function $\psi(z)$, Atangana-Baleanu Caputo fractional derivative order of ϕ satisfying the condition,

$$ {}_a^{ABC}D_z^{\phi}\psi(z) = \frac{G(\phi)}{1-\phi} \frac{d}{dz} \int_0^z \psi(\eta) E_{\phi}\left(\frac{\phi}{1-\phi} (z-\eta)^{\phi} \right) d\eta \, , for \; 0 < \phi < 1. \tag{8} $$

where $\mathrm{G}(\phi) = 1 - \phi + \frac{\phi}{\Gamma(\phi)}$ satisfied condition G(0)=G(1)=1.

Example. Let $\psi(t) = t$ and $\varphi = \frac{1}{2}$. Then the ABC fractional derivative is ${}_0^{ABC}D_t^{1/2}(t) = 2\, G(1/2)\, t\, E_{1/2,2}\left(-t^{1/2}\right)$, where $G\left(\frac{1}{2}\right) = 1 - \frac{1}{2} + \frac{1/2}{\Gamma(1/2)} = \frac{1}{2} + \frac{1}{2\sqrt{\pi}} \approx 0.5 + 0.2821 \approx 0.7821$.

Definition 2.8 ([7]). For function ϕ, Atangana-Baleanu Caputo fractional integral order of ϕ satisfying following condition for $0 < \phi < 1$;

$$ {}_0^{ABC}I_z^{\phi}\psi(z) = \frac{1-\phi}{G(\phi)}\psi(z) + \frac{\phi}{\Gamma(\phi)G(\phi)} \int_0^z \psi(\eta) \cdot (z-\eta)^{\phi-1} \, d\eta. \tag{9} $$

Example. For $\psi(z) = z$ and $\varphi = \frac{1}{2}$, the ABC fractional integral is ${}_0^{ABC}I_t^{1/2}(t) = \frac{t}{1+\frac{1}{\sqrt{\pi}}} \left[1 + \frac{4\sqrt{t}}{3\sqrt{\pi}}\right]$

3 Numerical Scheme

In this section, we develop a numerical SOFDE scheme for the ABC operator. The system is then applied to several examples. To derive the scheme, let us consider a general second-order fractional differential equation with an ABC operator of the form:

$$\begin{cases} D^{\phi}_{0,z}(D^{\phi}_{0,z}\psi(z)) = \xi(z,\psi(z)) \\ D^{\phi}\psi(0) = \psi_1, \psi(0) = \psi_0, \end{cases} \tag{10}$$

where $D^{\phi}_{0,z}$ is the ABC operator [8].

Applying the ABC fractional integral to both sides of the equation (10), we obtain

$$D^{\phi}_{0,z}\psi(z) = \frac{1-\phi}{G(\phi)}\xi(z,\psi(z)) + \frac{\phi}{\Gamma(\phi)G(\phi)}\int_0^z \xi(\eta,\psi(\eta))\cdot(z-\eta)^{\phi-1}\,d\eta + C$$

Using the initial condition, we get

$$= \psi_1 - \frac{1-\phi}{G(\phi)}\cdot\xi_0 + \frac{1-\phi}{G(\phi)}\xi(z,\psi(z)) + \frac{\phi}{G(\phi)}\cdot^{RL} I^{\phi}_z\xi(z,\psi(z)) \tag{11}$$

where $\xi_0 = \xi(0,\psi(0))$ and integrate again, we get

$$\begin{aligned} \psi(z) =& \psi_0 - \frac{(1-\phi)^2}{G(\phi)^2}\xi_0 - \frac{(1-\phi)\cdot z^{\phi}}{\Gamma(\phi)\cdot G(\phi)^2}\xi_0 + \frac{2\phi(1-\phi)}{G(\phi)^2}\cdot^{RL} I^{\phi}_z\xi(z,\psi(z)) \\ &+ \frac{\phi^2}{G(\phi)^2}\cdot^{RL} I^{2\phi}_z\xi(z,\psi(z)) + \frac{(1-\phi)^2}{G(\phi)^2}\cdot\xi(z,\psi(z)) + \frac{z^{\phi}}{\Gamma(\phi)G(\phi)}\cdot\psi_1. \end{aligned} \tag{12}$$

For $\mu = 0, 1, 2, ...$, we have

$$\begin{aligned} \psi(z_{\mu+1}) =& \psi_0 - \frac{(1-\phi)^2}{G(\phi)^2}\xi_0 - \frac{(1-\phi)\cdot z^{\phi}_{\mu}}{\Gamma(\phi)\cdot G(\phi)^2}\xi_0 + \frac{2\phi(1-\phi)}{G(\phi)^2}\cdot^{RL} I^{\phi}_z\xi(z,\psi(z)) \\ &+ \frac{\phi^2}{G(\phi)^2}\cdot^{RL} I^{2\phi}_z\xi(z,\psi(z)) + \frac{(1-\phi)^2}{G(\phi)^2}\cdot\xi(z_{\mu},\psi(z_{\mu})) + \frac{z^{\phi}_{\mu}}{\Gamma(\phi)G(\phi)}\cdot\psi_1 \end{aligned} \tag{13}$$

where

$$^{RL}I^{\phi}_z\xi(z,\psi(z)) = \frac{1}{\Gamma(\phi)}\int_0^{z_{\mu+1}} \xi(\eta,\psi(\eta))\cdot(z_{\mu+1}-\eta)^{\phi-1}\,d\eta$$

$$= \frac{1}{\Gamma(\phi)}\sum_{\omega=0}^{\mu}\int_{z_{\omega}}^{z_{\omega+1}} \xi(\eta,\psi(\eta))\cdot(z_{\mu+1}-\eta)^{\phi-1}\,d\eta \tag{14}$$

The function $\xi(\eta,\psi(\eta)$ integrating from z_{ω} to $z_{\omega+1}$. So, Lagrange's interpolation polynomial passing through [29], i.e., $(z_{\omega},\phi_{\omega})$ and $(z_{\omega+1},\phi_{\omega+1})$ is

$$\begin{aligned} \xi(\eta,\psi(\eta)) &= \frac{(\eta-z_{\omega+1})}{(z_{\omega}-z_{\omega+1})}\cdot\xi(z_{\omega},\psi(z_{\omega})) + \frac{(\eta-z_{\omega})}{(z_{\omega+1}-z_{\omega})}\cdot\xi(z_{\omega+1},\psi(z_{\omega+1})) \\ &= \frac{(\eta-z_{\omega})}{(z_{\omega+1}-z_{\omega})}\cdot\xi(z_{\omega+1},\psi(z_{\omega+1})) - \frac{(\eta-z_{\omega+1})}{(z_{\omega+1}-z_{\omega})}\cdot\xi(z_{\omega},\psi(z_{\omega})) \end{aligned}$$

Put Δz=$(z_{\omega+1}-z_{\omega})$

$$\xi(\eta,\psi(\eta)) = \frac{(\eta-z_{\omega})}{\Delta(z)}\cdot\xi(z_{\omega+1},\psi(z_{\omega+1})) - \frac{(\eta-z_{\omega+1})}{\Delta(z)}\cdot\xi(z_{\omega},\psi(z_{\omega})) \tag{15}$$

Using equations (14) and (15), we get

$$
\begin{aligned}
{}^{RL}I_z^{\phi}\xi(z,\psi(z)) &= \frac{1}{\Gamma(\phi)}\sum_{\omega=0}^{\mu}\left[\frac{\xi(z_{\omega+1},\psi(z_{\omega+1}))}{\Delta(z)}\int_{z_\omega}^{z_{\omega+1}}(\eta-z_\omega)\cdot(z_{m+1}-\eta)^{\phi-1}\,d\eta\right.\\
&\quad\left.-\frac{\xi(z_\omega,\psi(z_\omega))}{\Delta(z)}\int_{z_\omega}^{z_{\omega+1}}(\eta-z_{\omega+1})\cdot(z_{m+1}-\eta)^{\phi-1}\,d\eta\right]\\
&= \frac{1}{\Gamma(\phi)}\sum_{\omega=0}^{\mu}\left[\frac{\xi(z_{\omega+1},\psi(z_{\omega+1}))}{\Delta(z)}B_{\phi,\omega,1}-\frac{\xi(z_\omega,\psi(z_\omega))}{\Delta(z)}B_{\phi,\omega,2}\right] \qquad (16)
\end{aligned}
$$

Using

$$
B_{\phi,\omega,1}=\int_{z_\omega}^{z_{\omega+1}}(\eta-z_\omega)\cdot(z_{m+1}-\eta)^{\phi-1}\,d\eta
$$

$$
\therefore B_{\phi,\omega,1}=\frac{\Delta(z)^{\phi+1}}{\phi(\phi+1)}\left\{(\mu-\omega+1)^{\phi+1}-(\mu-\omega)^{\phi}\cdot(1+\phi+\mu-\omega)\right\} \qquad (17)
$$

and

$$
\begin{aligned}
B_{\phi,\omega,2} &= \int_{z_\omega}^{z_{\omega+1}}(\eta-z_{\omega+1})\cdot(z_{\mu+1}-\eta)^{\phi-1}\,d\eta\\
\therefore B_{\phi,\omega,2} &= \frac{\Delta(z)^{\phi+1}}{\phi(\phi+1)}\left\{(\mu-\omega+1)^{\phi}\cdot(\mu-\omega-\phi)-(\mu-\omega)^{\phi+1}\right\}
\end{aligned} \qquad (18)
$$

Using equations (17) and (18) in equation (16), we get

$$
\begin{aligned}
{}^{RL}I_z^{\phi}\xi(z,\psi(z)) &= \frac{\Delta(z)^{\phi+1}}{\Gamma(\phi+2)}\sum_{\omega=0}^{\mu}\left[\frac{\xi(z_{\omega+1},\psi(z_{\omega+1}))}{\Delta(z)}\right.\\
&\quad\cdot\left\{(\mu-\omega+1)^{\phi+1}-(\mu-\omega)^{\phi}\cdot(1+\phi+\mu-\omega)\right\}\\
&\quad\left.-\frac{\xi(z_\omega,\psi(z_\omega))}{\Delta(z)}\cdot\left\{(\mu-\omega+1)^{\phi}\cdot(\mu-\omega-\phi)-(\mu-\omega)^{\phi+1}\right\}\right]
\end{aligned} \qquad (19)
$$

Similarly,

$$
\begin{aligned}
{}^{RL}I_z^{2\phi}\xi(z,\psi(z)) &= \frac{\Delta(z)^{2\phi+1}}{\Gamma(2\phi+2)}\sum_{\omega=0}^{\mu}\left[\frac{\xi(z_{\omega+1},\psi(z_{\omega+1}))}{\Delta(z)}\right.\\
&\quad\cdot\left\{(\mu-\omega+1)^{2\phi+1}-(\mu-\omega)^{2\phi}\cdot(1+2\phi+\mu-\omega)\right\}\\
&\quad\left.-\frac{\xi(z_\omega,\psi(z_\omega))}{\Delta(z)}\left\{(\mu-\omega+1)^{2\phi}\cdot(\mu-\omega-2\phi)-(\mu-\omega)^{2\phi+1}\right\}\right]
\end{aligned} \qquad (20)
$$

Putting equations (19) and (20) in equation (13), we get

$$
\begin{aligned}
\psi(z_{\mu+1}) =& \psi_0+\frac{2\phi(1-\phi)}{G(\phi)^2}\cdot\frac{\Delta(z)^{\phi}}{\Gamma(\phi+2)}\sum_{\omega=0}^{\mu}[\xi(z_{\omega+1},\psi(z_{\omega+1}))\\
&\cdot\left\{(\mu-\omega+1)^{\phi+1}-(\mu-\omega)^{\phi}\cdot(1+\phi+\mu-\omega)\right\}\\
&-\xi(z_\omega,\psi(z_\omega))\cdot\left\{(\mu-\omega+1)^{\phi}\cdot(\mu-\omega-\phi)-(\mu-\omega)^{\phi+1}\right\}]\\
&+\frac{\phi^2}{G(\phi)^2}\cdot\frac{\Delta(z)^{2\phi}}{\Gamma(2\phi+2)}\sum_{\omega=0}^{\mu}[\xi(z_{\omega+1},\psi(z_{\omega+1}))\\
&\cdot\left\{(\mu-\omega+1)^{2\phi+1}-(\mu-\omega)^{2\phi}\cdot(1+2\phi+\mu-\omega)\right\}\\
&-\xi(z_\omega,\psi(z_\omega))\left\{(\mu-\omega+1)^{2\phi}\cdot(\mu-\omega-2\phi)-(\mu-\omega)^{2\phi+1}\right\}]\\
&+\frac{(1-\phi)^2}{G(\phi)^2}\cdot\xi(z_\mu,\psi(z_\mu))+\frac{z_\mu^{\phi}}{\Gamma(\phi)G(\phi)}\cdot\psi_1-\frac{(1-\phi)^2}{G(\phi)^2}\xi_0-\frac{(1-\phi)\cdot z_\mu^{\phi}}{\Gamma(\phi)\cdot G(\phi)^2}\xi_0
\end{aligned} \qquad (21)
$$

3.1 Stability and Convergence of Scheme

In this part, we show the stability and convergence of the numerical scheme solution [14]. Using equation (13)

$$\psi(z_{\mu+1}) = D + \frac{2\phi(1-\phi)}{G(\phi)^2} \cdot^{RL} I_z^{\phi}\xi(z,\psi(z)) + \frac{\phi^2}{G(\phi)^2} \cdot^{RL} I_z^{2\phi}\xi(z,\psi(z))$$

where ,

$$D = \psi_0 - \frac{(1-\phi)^2}{G(\phi)^2}\xi_0 - \frac{(1-\phi)\cdot z_\mu^{\phi}}{\Gamma(\phi)\cdot G(\phi)^2}\xi_0 + \frac{(1-\phi)^2}{G(\phi)^2}\cdot\xi(z_\mu,\psi(z_\mu)) + \frac{z_\mu^{\phi}}{\Gamma(\phi)G(\phi)}\cdot\psi_1$$

Now, we get

$$\psi(z_{\mu+1}) = D + \frac{2\phi(1-\phi)}{G(\phi)^2}\cdot\frac{1}{\Gamma(\phi)}\int_0^{z_{\mu+1}}\xi(\eta,\psi(\eta))\cdot(z_{\mu+1}-\eta)^{\phi-1}\,d\eta + \frac{\phi^2}{G(\phi)^2}\cdot\frac{1}{\Gamma(2\phi)}\int_0^{z_{\mu+1}}\xi(\eta,\psi(\eta))\cdot(z_{\mu+1}-\eta)^{2\phi-1}\,d\eta$$

$$\begin{aligned}\psi(z_{\mu+1}) &= D + \frac{2\phi(1-\phi)}{G(\phi)^2}\cdot\frac{1}{\Gamma(\phi)}\sum_{\omega=0}^{\mu}\int_{z_\omega}^{z_{\omega+1}}\xi(\eta,\psi(\eta))\cdot(z_{\mu+1}-\eta)^{\phi-1}\,d\eta \\ &+ \frac{\phi^2}{G(\phi)^2}\cdot\frac{1}{\Gamma(2\phi)}\sum_{\omega=0}^{\mu}\int_{z_\omega}^{z_{\omega+1}}\xi(\eta,\psi(\eta))\cdot(z_{\mu+1}-\eta)^{2\phi-1}\,d\eta \\ &= D + \frac{2\phi(1-\phi)}{G(\phi)^2}\cdot\frac{1}{\Gamma(\phi)}\sum_{\omega=0}^{\mu}\int_{z_\omega}^{z_{\omega+1}}\left\{P_{k1}(\eta) + \frac{(\eta-z_\omega)(\eta-z_{\omega+1})}{2!}\frac{\partial^2}{\partial\eta^2}[\xi(\eta,\psi(\eta))]_{\eta=\xi_\eta}\right\} \\ &\cdot(z_{\mu+1}-\eta)^{\phi-1}\,d\eta + \frac{\phi^2}{G(\phi)^2}\cdot\frac{1}{\Gamma(2\phi)}\sum_{\omega=0}^{\mu}\int_{z_\omega}^{z_{\omega+1}}\left\{P_{k2}(\eta) + \frac{(\eta-z_\omega)(\eta-z_{\omega+1})}{2!}\frac{\partial^2}{\partial\eta^2}[\xi(\eta,\psi(\eta))]_{\eta=\xi_\eta}\right\} \\ &\cdot(z_{\mu+1}-\eta)^{2\phi-1}\,d\eta\end{aligned}$$

$$\begin{aligned}\psi(z_{\mu+1}) = D + \frac{2\phi(1-\phi)}{\Gamma(\phi)G(\phi)^2}\sum_{\omega=0}^{\mu}\Bigg\{&\frac{\xi(x_{\omega+1},\psi_{\omega+1})}{\Delta z}\int_{z_\omega}^{z_{\omega+1}}(\eta-z_\omega)\cdot(z_{\mu+1}-\eta)^{\phi-1}\,d\eta - \frac{\xi(x_\omega,\psi_\omega)}{\Delta z} \\ &\int_{z_\omega}^{z_{\omega+1}}(\eta-z_{\omega+1})\cdot(z_{\mu+1}-\eta)^{\phi-1}\,d\eta\Bigg\} + \frac{\phi^2}{\Gamma(2\phi)G(\phi)^2}\sum_{\omega=0}^{\mu}\int_{z_\omega}^{z_{\omega+1}}\Bigg\{\frac{\xi(x_{\omega+1},\psi_{\omega+1})}{\Delta z} \\ &\int_{z_\omega}^{z_{\omega+1}}(\eta-z_\omega)\cdot(z_{\mu+1}-\eta)^{\phi-1}\,d\eta - \frac{\xi(x_\omega,\psi_\omega)}{\Delta z}\int_{z_\omega}^{z_{\omega+1}}(\eta-z_{\omega+1})\cdot(z_{\mu+1}-\eta)^{\phi-1}\,d\eta\Bigg\} + E \quad (22)\end{aligned}$$

where, $E = E_\mu^{\phi} + E_\mu^{2\phi}$ and error is given as

$$E_\mu^{\phi} = \frac{2\phi(1-\phi)}{\Gamma(\phi)G(\phi)^2}\sum_{\omega=0}^{\mu}\int_{z_\omega}^{z_{\omega+1}}\frac{(\eta-z_\omega)(\eta-z_{\omega+1})}{2!}\frac{\partial^2}{\partial\eta^2}[\xi(\eta,\psi(\eta))]_{\eta=\xi_\eta}(z_{\mu+1}-\eta)^{\phi-1}\,d\eta \quad (23)$$

$$E_\mu^{2\phi} = \frac{\phi^2}{\Gamma(2\phi)G(\phi)^2}\sum_{\omega=0}^{\mu}\int_{z_\omega}^{z_{\omega+1}}\frac{(\eta-z_\omega)(\eta-z_{\omega+1})}{2!}\frac{\partial^2}{\partial\eta^2}[\xi(\eta,\psi(\eta))]_{\eta=\xi_\eta}(z_{\mu+1}-\eta)^{2\phi-1}\,d\eta. \quad (24)$$

From equation (23), and the function $(\eta-z_w)(z_{\mu+1}-\eta)^{\phi-1}$ is positive in the interval $[z_\omega, z_{\omega+1}]$. By using mean value theorem for integral, there exists $\xi_\omega = [z_\omega, z_{\omega+1}]$ such that

$$\begin{aligned}E_\mu^{\phi} &= \frac{2\phi(1-\phi)}{\Gamma(\phi)G(\phi)^2}\sum_{\omega=0}^{\mu}\frac{\partial^2}{\partial^2\eta}[\xi(\eta,\psi(\eta))]_{\eta=\xi_\omega}\frac{(\xi_\omega-z_{\omega+1})}{2}\int_{z_\omega}^{z_{\omega+1}}(\eta-z_\omega)(z_{\mu+1}-\eta)^{\phi-1}\,d\eta \\ &= \frac{2\phi(1-\phi)}{\Gamma(\phi)G(\phi)^2}\sum_{\omega=0}^{\mu}\frac{\partial^2}{\partial\eta^2}[\xi(\eta,\psi(\eta))]_{\eta=\xi_\omega}\frac{(\xi_\omega-z_{\omega+1})}{2}\cdot B_{\phi,\omega,1}\end{aligned}$$

For absolute value of E_μ^ϕ

$$B_{\phi,\omega,1} = \frac{\Delta(z)^{\phi+1}}{\phi(\phi+1)}\left\{(\mu-\omega+1)^{\phi+1} - (\mu-\omega)^\phi \cdot (1+\phi+\mu-\omega)\right\}$$

$$|E_\mu^\phi| < \frac{\phi(1-\phi)\Delta(z)^{\phi+2}}{\Gamma(\phi+2)G(\phi)^2} \max_{[0,z_\mu+1]} \left|\frac{\partial^2}{\partial\eta^2}\xi(\eta,\psi(\eta))\right| \cdot \left|\sum_{\omega=0}^{\mu}\left\{(\mu-\omega+1)^{\phi+1} - (\mu-\omega)^\phi \cdot (1+\phi+\mu-\omega)\right\}\right| \tag{25}$$

Taking only the right-hand side of the summation, we get

$$(\mu-\omega+1)^{\phi+1} - (\mu-\omega)^\phi \cdot (1+\phi+\mu-\omega) = (\mu-\omega+1)\{(\mu-\omega+1)^\phi - (\mu-\omega)^\phi\} - \phi(\mu-\omega)^\phi$$

$$\begin{aligned} &< (\mu-\omega+1)\{(\mu-\omega+1)^\phi - (\mu-\omega)^\phi\} - \phi(\mu)^\phi \\ &< (\mu-\omega+1)\{(\mu+1)^\phi - (\mu)^\phi\} - \phi(\mu)^\phi \\ &< (\mu+1)\{(\mu+1)^\phi - (\mu)^\phi\} - \phi(\mu)^\phi \end{aligned}$$

As we know,

$$\sum_{\omega=0}^{\mu}(\mu+1)\{(\mu+1)^\phi - (\mu)^\phi\} - \phi(\mu)^\phi = \mu[(\mu+1)\{(\mu+1)^\phi - (\mu)^\phi\} - \phi(\mu)^\phi] \tag{26}$$

In equation (25)

$$|E_\mu^\phi| < \frac{\phi(1-\phi)(\Delta z)^{\phi+2}}{\Gamma(\phi+2)G(\phi)^2} \max_{[0,z_{\mu+1}]} \left|\frac{\partial^2}{\partial\eta^2}\xi(\eta,\psi(\eta))\right| \cdot \mu[(\mu+1)\{(\mu+1)^\phi - (\mu)^\phi\} - \phi(\mu)^\phi] \tag{27}$$

Apply a similar process to the equation (24).

$$|E_\mu^{2\phi}| < \frac{\phi^2(\Delta z)^{2\phi+2}}{2\Gamma(2\phi+2)G(\phi)^2} \max_{[0,z_{\mu+1}]} \left|\frac{\partial^2}{\partial\eta^2}[\xi(\eta,\psi(\eta))]\right| \cdot \mu[(\mu+1)\{(\mu+1)^{2\phi} - (\mu)^{2\phi}\} - \phi(\mu)^{2\phi}] \tag{28}$$

Putting in equations (27) and (28) for $E = E_\mu^\phi + E_\mu^{2\phi}$, then we get

$$\begin{aligned} |E| < \frac{\mu\phi(\Delta z)^{\phi+2}}{G(\phi)^2} \max_{[0,z_{\mu+1}]} \left|\frac{\partial^2}{\partial\eta^2}[\xi(\eta,\psi(\eta))]\right| \Bigg\{ &\frac{1-\phi}{\Gamma(\phi+2)}[(\mu+1)\{(\mu+1)^\phi - (\mu)^\phi\} - \phi(\mu)^\phi] \\ &+ \frac{\phi(\Delta z)^\phi}{2\Gamma(2\phi+2)}[(\mu+1)\{(\mu+1)^{2\phi} - (\mu)^{2\phi}\} - 2\phi(\mu)^{2\phi}]\Bigg\} = O(\Delta z^{\phi+2}) \end{aligned} \tag{29}$$

When the error E between the exact and approximate solutions is bounded [12], the errors of the scheme do not grow uncontrollably [13], which implies stability [3, 5, 28]. Additionally, the error tends to zero as $\Delta z \to 0$, indicating that the scheme is convergent [6, 27]. Hence, the scheme has both convergence and stability [4].

4 Applications

The numerical scheme described above is used to solve fractional differential equations with initial conditions [26]. Subsequently, a detailed discussion of the solution is presented.

Example 4.1. Consider the second-order fractional differential equation [9, 32]:

$$\begin{aligned} &D_{0,z}^\phi D_{0,z}^\phi \psi(z) = z \quad for\ z > 0, \\ &D_{0,z}^\phi \psi(0) = 0,\ \psi(0) = 0. \end{aligned} \tag{30}$$

The exact solution is obtained by using the ABC operator, integrating twice:

$$\psi(z) = \frac{(1-\phi)^2}{G(\phi)^2} \cdot z + \frac{2\phi(1-\phi)}{G(\phi)^2 \cdot \Gamma(\phi+2)} \cdot z^{\phi+1} + \frac{\phi^2}{G(\phi)^2 \cdot \Gamma(2\phi+2)} \cdot z^{2\phi+1} \tag{31}$$

Now, we find some solutions to equation (30) according to the scheme and show them in the table. Tables 1 and 2 present the numerical approximation of Eq. (30) at $z = 10$ for a range of fractional orders ϕ and various step sizes (Δz). Table 2 continues the results presented in Table 1. The tables compare the approximate solutions obtained using the proposed scheme with the exact solutions and present the corresponding absolute errors for $\phi \in [0.1, 1]$. The numerical results show that the method achieves high accuracy, with errors decreasing as the step size is refined.In particular, for $z = \frac{1}{270}$, the error decreases from 3.6187×10^{-3} at $\phi = 0.1$ to 2.2737×10^{-13} at $\phi = 1$, demonstrating the strong convergence of the scheme. Figures 1–2 provide a comprehensive graphical representation of the numerical behavior of Eq. (30) for different fractional orders and values of z. Figure 1(a) illustrates the evolution of the solution for ϕ ranging from 0.1 to 0.9. The three-dimensional graphs in Figures 1(e) and 1(b) compare approximate and exact solutions for $\phi = 0.5$, while Figures 1(c) and 1(d) show similar comparisons for $\phi = 0.7$ and $\phi = 1$, using a uniform step size of 0.1. These visualizations highlight the ability of the method to accurately reproduce both the qualitative and quantitative behavior of the exact solution. Figures 1(e) and 1(f) depict the numerical solution in the ϕ–z plane, illustrating the smoothness and continuity of the surface. The monotonic increase in the solution with respect to ϕ further reflects the stability and robustness of the method. Figures 2(a) and 2(b) present the corresponding error surfaces, emphasizing the accuracy and consistent convergence of the scheme as the step size decreases. Figures 2(c) and 2(d) analyze the dependence of the approximation error on both fractional order ϕ and step size Δz, revealing the sensitivity of the method to variations in these parameters. The results show that the error decreases significantly as Δz becomes smaller and that the sensitivity to ϕ is more pronounced at finer resolutions. Taken together, all figures provide a coherent visualization of the precision, convergence, and robustness of the method for solving Eq. (30).

Table 1: A comparison of the exact and approximate solutions is presented for various step sizes Δz and fractional orders ϕ at $z = 10$ (Part 1).

Δz	ϕ value					
	0.1	**0.2**	**0.3**	**0.4**	**0.5**	**0.6**
$\frac{1}{10}$	12.4582	16.5091	22.706	31.6829	43.9274	59.7048
$\frac{1}{30}$	12.5234	16.5691	22.7536	31.7223	43.9546	59.7214
$\frac{1}{90}$	12.5451	16.5891	22.7706	31.7354	43.9637	59.7269
$\frac{1}{270}$	12.5523	16.5957	22.7763	31.7398	43.9637	59.7287
Exact value	12.5559	16.5991	22.7791	31.742	43.9683	59.7296
Last Error	0.0036187	0.003331	0.0028336	0.0021897	0.0015138	0.00091915

Table 2: Remaining comparison of solution for $z = 10$ (Part 2).

Δz	ϕ value			
	0.7	**0.8**	**0.9**	**1**
$\frac{1}{10}$	79.2258	102.8999	131.5672	166.667
$\frac{1}{30}$	79.2344	102.9033	131.5679	166.667
$\frac{1}{90}$	79.2372	103.9044	131.5682	166.667
$\frac{1}{270}$	79.2381	102.9048	131.5683	166.667
Exact Value	79.2386	102.905	131.5683	166.667
Last Error	0.00047323	0.00018824	4.1894E-05	2.2737E-13

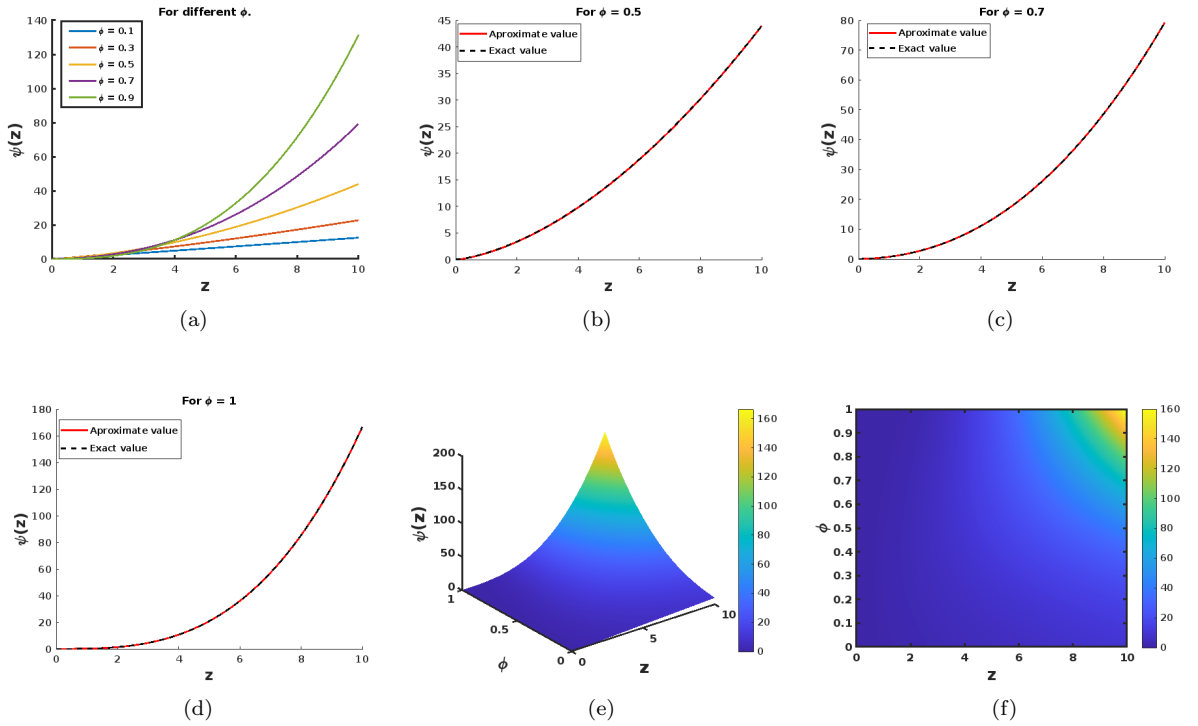

Figure 1: (a) Approximate solutions for various values of ϕ. (b) Comparison between the approximate and exact solutions at $\phi = 0.5$ with a step size of 0.1. (c) Comparison between the approximate and exact solutions at $\phi = 0.7$ with a step size of 0.1. (d) Comparison between the approximate and exact solutions at $\phi = 1.0$ with a step size of 0.1. (e) Three-dimensional plot of the numerical solution with respect to ϕ and z. (f) Two-dimensional plot of the numerical solution with respect to ϕ and z.

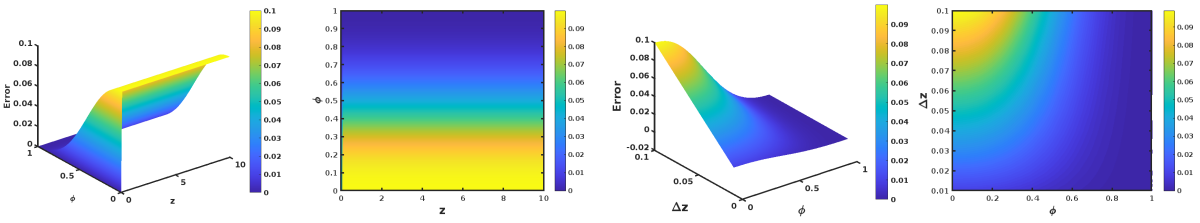

Figure 2: (a) 3D graph for error analysis with ϕ and z. and (b) 2D graph for error analysis with ϕ and z. (c) 3D graph for error analysis with ϕ and Δz. (d) 2D graph for error analysis with ϕ and Δz.

Example 4.2. Consider the second-order differential equation [9, 32]:

$$\begin{aligned} D^{\phi}_{0,z} D^{\phi}_{0,z} \psi(z) &= \sin z \quad \text{for } z > 0, \\ D^{\phi}_{0,z} \psi(0) &= 0, \quad \psi(0) = 0. \end{aligned} \tag{32}$$

The exact solution of this equation is obtained by integrating twice:

$$\psi(z) = \frac{(1-\phi)^2}{G(\phi)^2} sin(z) + \frac{2\phi(1-\phi)}{G(\phi)^2} z^{\phi+1} E_{2,\phi+2}(-z^2) + \frac{\phi^2}{G(\phi)^2} z^{2\phi+1} E_{2,2\phi+2}(-z^2). \tag{33}$$

When $z = 50$ and $\phi = 1$, the solutions of equation (32) are obtained and shown in the table:
Tables 3 and 4 present the numerical solution of Equation (32). Table 3 focuses on the effect of the step size

(Δz) on the approximate solution, comparing the exact solution with the approximate solution obtained using the numerical scheme for $\phi = 1$ and $z = 50$. The table also provides the error between the exact and approximate solutions. Similarly, Table 4 shows the solutions for different fractional orders ϕ at a fixed value of $z = 50$. The table presents the exact solution and the approximate solution for ϕ values ranging from 0.1 to 1, along with the corresponding errors. Figure 3(a) illustrates how the error between the approximate and exact solutions evolve as the step size decreases. By plotting the solutions for different values of ϕ, Figures 3(b) and 3(c) effectively show how sensitive the solution is to changes in this parameter, which can be useful for understanding the dynamics of the modeled system. The value of the solution $\psi(z)$ is maximum at the highest value of ϕ; if ϕ decreases continuously, the solution also decreases. As shown in Figures 3(d) and 4(a), the solution increases smoothly as the order of the fractional derivative increases. Furthermore, according to Figures 4(b) and 4(c), the error is maximum at the minimum ϕ, but for any value of z or larger step sizes, the error remains consistent.

Table 3: Solution of Eq. (32) for different Δz.

Δz	**Exact solution**	**Approximate solution**	**Error**
1/10	50.2624	50.2205	0.041892
1/30	50.2624	50.2577	0.004654
1/90	50.2624	50.2619	0.0005171
1/270	50.2624	50.2623	0.000057456

Table 4: Solutions of Eq. (32) at $z = 50$ for Various Fractional Orders ϕ

ϕ value	Δz					
	$\frac{1}{10}$	$\frac{1}{30}$	$\frac{1}{90}$	$\frac{1}{270}$	**Exact solution**	**Last error**
0.1	-0.444	-0.38248	-0.36167	-0.3547	-0.35121	0.0034901
0.2	-0.60466	-0.54816	-0.52902	-0.5226	-0.51939	0.0032124
0.3	-0.8111	-0.76326	-0.744	-0.74155	-0.73882	0.0027324
0.4	-0.95042	-0.91369	-0.90116	-0.89694	-0.89483	0.0021111
0.5	-0.77546	-0.75016	-0.7415	-0.73859	-0.73713	0.0014593
0.6	0.18234	0.19819	0.2035	0.20527	0.20616	0.00088647
0.7	2.824	2.8341	2.8371	2.838	2.8385	0.00045971
0.8	8.9565	8.9663	8.9682	8.9696	8.9688	0.00019182
0.9	22.261	22.2783	22.2803	22.2806	22.2807	6.9175e-05

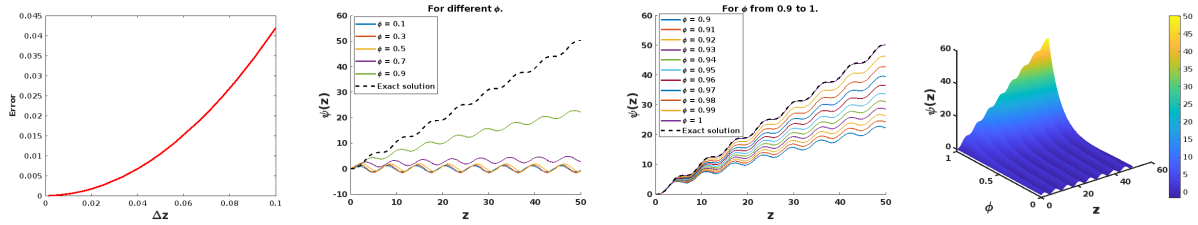

(a) (b) (c) (d)

Figure 3: (a) shows the relation between step size and error. (b) demonstrate solutions for various values of ϕ from 0.1 to 0.9 as well as exact solution ($\phi = 1$). (c) demonstrates Numerical solutions for various values of ϕ from 0.9 to 1 as well as exact solution ($\phi = 1$). (d) 3D visualization of solution with respect to ϕ and z.

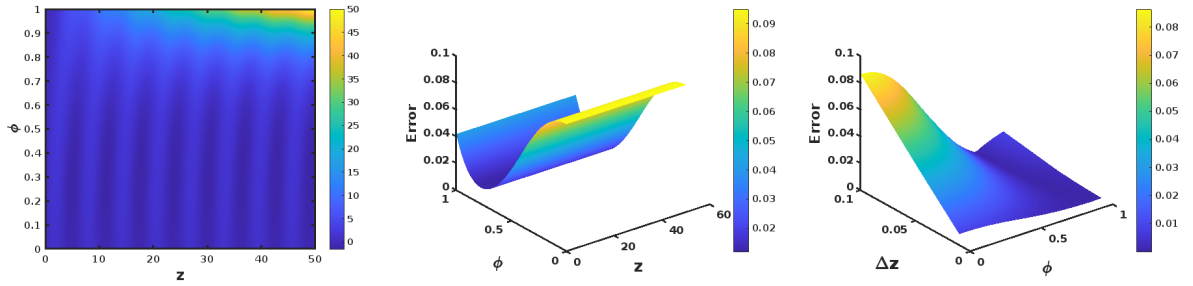

(a) (b) (c)

Figure 4: (a) 2D behavior of solution with respect to ϕ and z. (b) shows the error according to ϕ and z. (c) error w.r.t step size and the order of the derivative.

Example 4.3. Let us consider a non-homogeneous second-order fractional differential equation with initial condition [9]:

$$\begin{aligned} &D^{\phi}_{0,z} D^{\phi}_{0,z} \psi(z) = e^z \quad for\ z > 0, \\ &D^{\phi}_{0,z} \psi(0) = \frac{1}{2},\ \psi(0) = 0. \end{aligned} \tag{34}$$

where $0 < \phi < 1$ and $D^{\phi}_{0,z}$ is ABC operator.

The exact solution of an equation is

$$\psi(z) = \frac{e^z}{G(\phi)^2} - \frac{2\phi - \phi^2}{G(\phi)^2} + \frac{1-\phi}{2G(\phi)} + \frac{z^{\phi}}{2G(\phi)\cdot\Gamma(\phi)} - \frac{\phi \cdot z^{\phi}}{G(\phi)^2 \cdot \Gamma(\phi)} \tag{35}$$

Also, when ϕ=1, the exact solution of differential equation (34) is obtained by using the above scheme for ABC fractional derivative, and we show the result in tables.

Tables 5, 6, and 7 present the numerical solution of Eq. (34). Table 5 focuses on the effect of the step size on the solution at $\phi = 1$ and shows how the error decreases as the step size (Δz) becomes smaller, indicating that the numerical approximation becomes more accurate. This table also provides a comparison of the exact and approximate solutions. Table 6 compares the solutions for different ϕ values at a fixed $z = 10$, demonstrating how the solution varies with different step sizes and ϕ values, as well as how closely it matches the exact solution. Table 7 shows the approximate values for $\phi = 0.99$ for different values of z, which are similar to those in Table 5. It also compares solutions at different step sizes and various values of z (i.e., 8, 10, and 12). Table 5 illustrates how smaller step sizes reduce the error and how the solutions compare to exact values. Each table helps in understanding the accuracy of the numerical solutions for different step sizes and parameters by demonstrating convergence to the exact solution as the step size decreases.

Figures 5–7 provide comprehensive visual representations of the numerical solution to Equation (34), demonstrating the efficacy of the proposed method in approximating the exact solution for various values of the fractional order ϕ and the independent variable z. Each figure offers a distinct perspective on the solution's behavior. Figures 5(a) and 5(b) provide a visual comparison of the exact and approximate solutions. The approximate solution is nearly identical to the exact solution for $\phi = 1$ in Fig. 5(a) and for $\phi = 0.99$ in Fig. 5(b) at the minimum step size $\Delta z = 0.1$. Figure 6 illustrates the behavior of the numerical solution with respect to the independent variable z and the fractional order ϕ in different dimensional plots. Figure 5(c) shows the approximate solution $\psi(z)$ for various values of ϕ, demonstrating how the solution changes with ϕ across the range of z. Figures 6(a) and 6(b) show that the solution continuously increases as ϕ is increased until it reaches the midpoint, then decreases from the midpoint to 1. Figures 6(c) and 7(a) show the error between the approximate and exact solutions with respect to ϕ and z for a step size of $\Delta z = \frac{1}{90}$, highlighting the method's accuracy and convergence. The error surfaces demonstrate that the

method achieves high accuracy, with errors decreasing as the step size decreases. Additionally, the error increases when the value of the variable z increases or when ϕ decreases, as illustrated in the figures. Figure 7 illustrates how the error behavior varies with different values of ϕ and step sizes Δz for the independent variable $z = 10$. As shown, the error is significantly influenced by the choice of step size. The figures further highlight that using a smaller step size minimizes the error, making it nearly negligible. Figure 7(b) illustrates that the error decreases smoothly as the step size decreases or as the fractional order ϕ increases from 0 to 1. This trend is also evident in Figure 7(c). Notably, the error reaches its maximum when the step size is at its largest.

Table 5: Solution of Eq.(34) for ϕ=1 and z=10.

Δz	**Exact solution**	**Approximate solution**	**Error**
1/10	22020.4658	22038.7712	18.3054
1/30	22020.4658	22022.4877	2.0219
1/90	22020.4658	22020.6867	0.22094
1/270	22020.4658	22020.4891	0.023314
1/810	22020.4658	22020.468	0.002179
1/2430	22020.4658	22020.4659	0.00010493

Table 6: Solution of Eq.(34) for $z = 10$.

Δz	ϕ value				
	0.5	**0.6**	**0.7**	**0.8**	**0.9**
1/10	35174.2789	33670.2276	31025.4847	27900.2925	24804.9803
1/30	35716.895	33990.4914	31180.1645	27950.2852	24802.2863
1/90	35910.4026	34106.977	31239.0032	27972.411	24805.6644
1/270	35976.3535	34146.9129	31259.4376	27980.3977	24807.2663
1/810	35998.5001	34160.3491	31266.3409	27983.128	24807.8531
Exact value	36009.017	34166.0533	31268.4568	27983.0993	24807.1218

Table 7: Solution of Eq.(34) for $\phi = 0.99$.

Δz	z value		
	8	**10**	**12**
1/10	3013.3596	22295.8862	164781.4657
1/30	3011.1816	22279.551	164660.5137
1/90	3010.9512	22277.7769	164647.3319
1/270	3010.9294	22277.5931	164645.951
1/810	3010.9283	22277.5771	164645.8255
Exact value	3010.8241	22277.4352	164645.6423

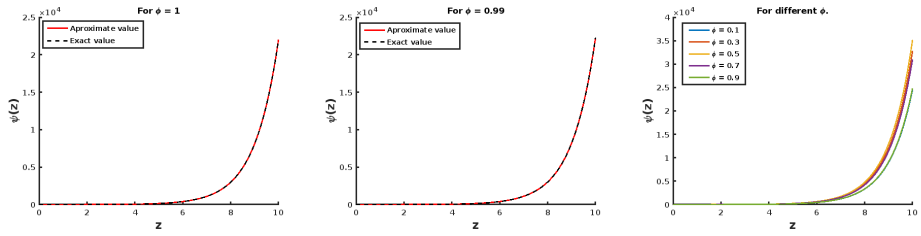

(a) (b) (c)

Figure 5: (a) Comparison of the exact and approximate solutions at $\phi = 1$. (b) Comparison of the exact and approximate solutions at $\phi = 0.99$.(c) Approximate solutions for various values of ϕ.

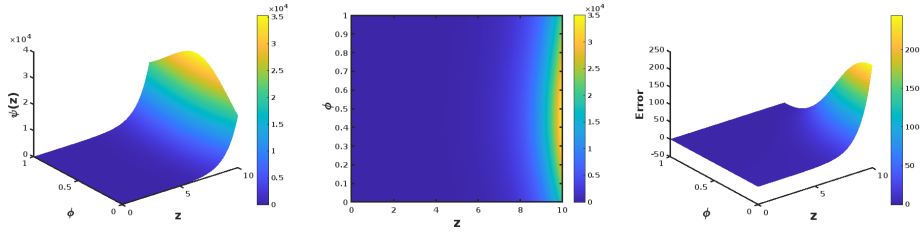

(a) (b) (c)

Figure 6: (a) 3D graph of the numerical solution with respect to ϕ and z. (b) 2D graph of the numerical solution with respect to ϕ and z. (c) 3D graph for error analysis with ϕ and z.

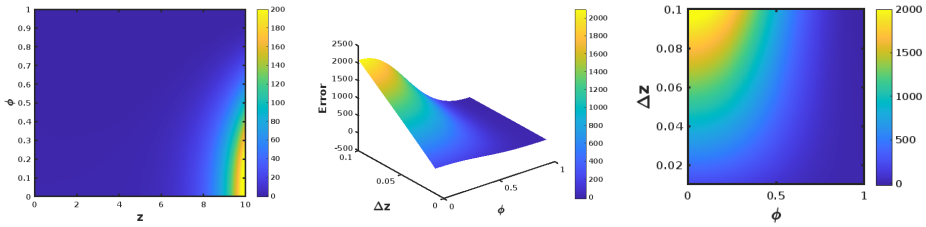

(a) (b) (c)

Figure 7: (a) 2D graph for error analysis with ϕ and z. (b) 3D graph for error analysis with ϕ and Δz. (b) 2D graph for error analysis with ϕ and Δz.

5 Conclusion

In this work, a robust numerical scheme based on Lagrange polynomial interpolation combined with the Atangana–Baleanu (ABC) fractional derivative has been successfully developed and applied to solve second-order fractional differential equations (SOFDEs). The proposed method provides accurate and computationally efficient approximate solutions, offering a practical approach for problems where analytical solutions are difficult or impossible to obtain. The numerical experiments consistently demonstrate the effectiveness of the scheme. The tabulated results and graphical illustrations confirm that the approximate solutions closely match the exact solutions, with the error decreasing significantly as the step size Δz is refined and the fractional order ϕ increases. The observed error behavior further highlights the stability and reliability of the proposed approach, showing that appropriate parameter selection greatly enhances accuracy. Overall, the simplicity, efficiency, and precision of the method underscore its potential as a valuable tool for solving a broad class of SOFDEs and suggest promising directions for extending the scheme to more complex fractional models in future research.

Acknowledgements. Jeevan Kafle acknowledges the Research Directorate, Rector Office, Tribhuvan University, Kathmandu, Nepal for the financial support through Major Research Grant. Shankar Pariyar expresses gratitude to the University Grants Commission (UGC), Nepal, for providing financial support through the PhD fellowship (Award No. PhD-2025/26-S&T-13).

References

[1] Ameen, I. (2017). *Fractional calculus: Numerical methods and SIR models* (Doctoral dissertation). University of Padova.

[2] Bruno, C. (2023). Turbulence and mixing. In *Airbreathing hypersonic propulsion: An introduction* (pp. 143–197). Springer Nature Singapore.

[3] Choudhary, R., Singh, S., Das, P., and Kumar, D. (2024). A higher-order stable numerical approximation for the time-fractional non-linear Kuramoto–Sivashinsky equation based on a quintic spline. *Mathematical Methods in the Applied Sciences*, 1–23. https://doi.org/10.1002/mma.9778

[4] Das, P. (2019). A posteriori-based convergence analysis for a nonlinear singularly perturbed system of delay differential equations on an adaptive mesh. *Numerical Algorithms*, 81, 465–487.

[5] Das, P. (2018). A higher-order difference method for singularly perturbed parabolic partial differential equations. *Journal of Difference Equations and Applications*, 24(3), 452–477.

[6] Das, P., Rana, S., and Ramos, H. (2022). Approximate solutions of a class of fractional-order nonlinear Volterra integro-differential initial- and boundary-value problems of the first kind and their convergence analysis. *Journal of Computational and Applied Mathematics*, 404, 113116.

[7] Deressa, C. T. (2022). On the chaotic nature of the Rabinovich system through Caputo and Atangana–Baleanu–Caputo fractional derivatives. *Advances in Continuous and Discrete Models*, 2022(1), 1–30.

[8] Diethelm, K. (2010). *The analysis of fractional differential equations*. Springer-Verlag. https://doi.org/10.1007/978-3-642-14574-2.

[9] Ilie, M., Biazar, J., and Ayati, Z. (2018). General solution of second-order fractional differential equations. *International Journal of Applied Mathematical Research*, 7(2), 56–61.

[10] Khan, H., Shah, R., Kumam, P., Baleanu, D., and Arif, M. (2020). Laplace decomposition for solving nonlinear systems of fractional-order partial differential equations. *Advances in Difference Equations*, 2020, 1–18.

[11] Kisela, T. (2008). Fractional differential equations and their applications. *Faculty of Mechanical Engineering, Institute of Mathematics*.

[12] Kumar, S., Das, P., and Kumar, K. (2024). Adaptive mesh-based efficient approximations for Darcy-scale precipitation–dissolution models in porous media. *International Journal for Numerical Methods in Fluids*, 96, 1415–1444.

[13] Kumar, S., Ishwariya, R., and Das, P. (2024). Impact of mixed boundary conditions and non-smooth data on layer-originated non-premixed combustion problems: Higher-order convergence analysis. *Studies in Applied Mathematics*. https://doi.org/10.1111/sapm.12763

[14] Kumar, K., Podila, P. C., Das, P., and Ramos, H. (2021). A graded mesh refinement approach for boundary-layer originated singularly perturbed time-delayed parabolic convection–diffusion problems. *Mathematical Methods in the Applied Sciences, 44*, 12332–12350.

[15] Lazarevic, M. P., Rapaic, M. R., Sekara, T. B., Mladenov, V., and Mastorakis, N. (2014). Introduction to fractional calculus with brief historical background. In *Advanced topics on applications of fractional calculus on control problems, system stability, and modeling*, 3–16. Springer.

[16] Li, C., Qian, D., and Chen, Y. (2011). On Riemann–Liouville and Caputo derivatives. *Discrete Dynamics in Nature and Society*, 2011, 1–15.

[17] Pandey, H. R., Phaijoo, G. R., and Gurung, D. B. (2024). A comprehensive study of fractional-order derivatives and their interplay with basic functions. *Journal of Nepal Mathematical Society*, 6(2), 38–52.

[18] Pariyar, S., Lamichhane, B. P., and Kafle, J. (2025). A time-fractional advection–diffusion approach to air pollution: Modeling and analyzing pollutant dispersion dynamics. *Partial Differential Equations in Applied Mathematics*, 14, 101149.

[19] Pariyar, S., and Kafle, J. (2022). Approximation solutions for solving some special functions of fractional calculus via Caputo–Fabrizio sense. *Nepal Journal of Mathematical Sciences*, 3(2), 1–10.

[20] Pariyar, S., and Kafle, J. (2023). Caputo–Fabrizio approach to numerical fractional derivatives. *BIBECHANA*, 20(2), 126–133.

[21] Pariyar, S., and Kafle, J. (2024). Generalizing the Mittag–Leffler function for fractional differentiation and numerical computation. *The Nepali Mathematical Sciences Report*, 41(1), 1–14.

[22] Pariyar, S., and Kafle, J. (2025). Fractional advection–diffusion equation with variable diffusivity: Pollutant effects using Adomian decomposition method. *Applied Mathematics E-Notes, 25*, 275–285.

[23] Podlubny, I., Magin, R. L., and Trymorush, I. (2017). Historical survey: Niels Henrik Abel and the birth of fractional calculus. *Fractional Calculus and Applied Analysis*, 20(2), 307–336.

[24] Ross, B. (1977). The development of fractional calculus 1695–1900. *Historia Mathematica*, 4, 75–89.

[25] Sabermahani, S., Ordokhani, Y., and Yousefi, S. A. (2018). Numerical approach based on fractional-order Lagrange polynomials for solving a class of fractional differential equations. *Computational and Applied Mathematics, 37*(3), 3846–3868.

[26] Saini, S., Das, P., and Kumar, S. (2023). Computational cost reduction for coupled systems of multiple-scale reaction–diffusion problems with mixed-type boundary conditions having boundary layers. *Revista de la Real Academia de Ciencias Exactas, Físicas y Naturales, Serie A: Matemáticas, 117*, 66.

[27] Saini, S., Das, P., and Kumar, S. (2024). Parameter-uniform higher-order numerical treatment for singularly perturbed Robin-type parabolic reaction–diffusion multiple-scale problems with large delay in time. *Applied Numerical Mathematics*, 196, 1–21. https://doi.org/10.1016/j.apnum.2023.10.003

[28] Santra, S., Mohapatra, J., Das, P., and Choudhuri, D. (2023). Higher-order approximations for fractional-order integro-parabolic partial differential equations on an adaptive mesh with error analysis. *Computers and Mathematics with Applications*, 150, 87–101.

[29] Shiromani, R., Shanthi, V., and Das, P. (2023). A higher-order hybrid numerical approximation for a class of singularly perturbed two-dimensional convection–diffusion elliptic problems with non-smooth convection and source terms. *Computers and Mathematics with Applications*, 142, 9–30.

[30] Srivastava, H. M. (2000). Review of *Fractional Differential Equations* by I. Podlubny. *Applied Mechanics Reviews*, 53(5), B51.

[31] Srivastava, H. M., Nain, A. K., Vats, R. K., and Das, P. (2023). A theoretical study of the fractional-order p-Laplacian nonlinear Hadamard-type turbulent flow models having Ulam–Hyers stability. *Revista de la Real Academia de Ciencias Exactas, Físicas y Naturales, Serie A: Matemáticas*, 117, 160.

[32] Toufik, M., and Atangana, A. (2017). New numerical approximation of fractional derivative with non-local and non-singular kernel: Application to chaotic models. *European Physical Journal Plus*, 132, 1–16.